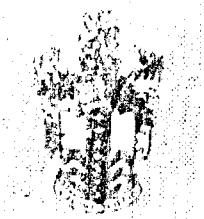

# RSRE
# MEMORANDUM No. 4129

# ROYAL SIGNALS & RADAR ESTABLISHMENT





## A THEORETICAL AND EXPERIMENTAL INVESTIGATION OF LINEAR AND NONLINEAR FOCUSSING CHIRPED OPTICAL DIFFRACTION GRATINGS

Authors: M F Lewis and C L West

ROYAL SIGNALS AND RADAR ESTABLISHMENT

MEMORANDUM NUMBER 4129

TITLE: A THEORETICAL AND EXPERIMENTAL INVESTIGATION OF LINEAR AND NONLINEAR FOCUSSING CHIRPED OPTICAL DIFFRACTION GRATINGS

AUTHORS: M F Lewis and C L West

DATE: June 1988

## SUMMARY

In the past the focussing properties of chirped grating structures have been investigated in various disciplines including optics, acousto-optics and acoustics. In this paper we present the results of a detailed theoretical and experimental study of one such structure, namely the chirped optical diffraction grating, although many of the conclusions are of more general validity. We derive some useful fundamental properties of such focussing gratings, and show that to first order their behaviour is similar to that of various other classical components such as focussing lenses, grating spectrometers, and matched filters for chirped waveforms. However we also describe a fascinating range of second-order differences in behaviour, for example concerning the physical locations of the multiple foci, and the sidelobe structures within and perpendicular to the focal plane. For devices of large numerical aperture we demonstrate the advantages of using a non-linear chirp grating structure, e.g. for sidelobe suppression in the focal plane, and point out that surface acoustic wave (SAW) techniques can be used to generate the non-linear chirp waveforms necessary to implement such gratings in acousto-optic devices.

## 1. INTRODUCTION

Chirped gratings are quasi-periodic structures in which the periodicity varies slowly with position, usually in a monotonic fashion, and often linearly. The focussing properties of such structures have long been recognised, the most familiar being the (2-dimensional) zone plate lens, with its excessive chromatic aberration [1]. Probably less familiar is the exploitation of this focussing phenomenon in the optical processing of synthetic aperture radar (SAR) data [2]. In acousto-optics, chirped (acoustic) gratings have demonstrated matched filtering in pulse compression radar [3,4,5], and a travelling lens capability for use in a high-speed high-resolution scanner [6]. Focussing chirp structures have also been studied in the planar technologies of integrated optics [7] and surface acoustic waves, SAW. In the latter work the 'chromatic aberration' of a slanted chirped SAW transducer was exploited to perform r.f. spectrum analysis [8,9]. All these studies and applications exploit the first-order focussing properties of linearly chirped structures. In the present paper we extend this work to include various second-order effects such as the detailed sidelobe structure in the vicinity of the focus, and the use of nonlinear chirp functions to improve the overall performance. Indeed in writing this paper we have found it most convenient to begin by deducing the ideal non-linear chirp pattern which produces a 'perfect' focus, and to which the linear chirp function is an approximation. The focussing properties of such an ideal structure are calculated and compared with those of the linear chirp pattern. In the later sections this comparison is verified by detailed measurements on the corresponding linearly and nonlinearly chirped optical diffraction gratings

## 2. FUNDAMENTAL PROPERTIES OF CHIRPED GRATINGS

A chirped optical diffraction grating is shown schematically in Figure 1(a) and is seen to resemble closely a single sided one-dimensional zone-plate lens. A minor difference concerns the slit-width, W. In a zone-plate lens W is usually varied to keep the mark/space ratio constant, as this allows an equal intensity through each zone. In a one-dimensional grating this is achieved by keeping W constant, and, in the discussion below, it is assumed that W is sufficiently small (relative to the optical wavelength, $\lambda$) to allow diffraction through a wide range of angles. We define the focus as being perfect if the contributions from all slits add constructively at a focal point, F, when the grating is illuminated by a plane wave of wavelength, $\lambda$. If $L_n$ is the optical path length from the $n^{th}$ slit to the focus, the condition for a perfect focus to occur under normal illumination is that the $L_n$ in Figure 1 differ by integral numbers of wavelengths, $\lambda$. Assuming for simplicity that the zeroth source is in line with the focus, F, all possible differential pathlengths from 0 to $N\lambda$ are included if

$$L_n = f + n\lambda \tag{1}$$

where n represents the set of positive integers from 0 to N. From Figure 1

$$L_n^2 = f^2 + Y_n^2 \tag{2}$$

combining Eqs (1) and (2) gives

$$Y_n = \pm\left[2fn\lambda + n^2\lambda^2\right]^{\frac{1}{2}} \tag{3}$$

where only (say) the positive square root is employed in a single-sided chirp grating. Eq (3) is often approximated by the *linear chirp* formula,

$$Y_n = \left[2fn\lambda\right]^{\frac{1}{2}} \tag{4}$$

These formulae are analogous to those obtaining for a classical circularly-symmetric zone-plate lens [1]. It may be noted that Eq (4) is also satisfied if f is reduced by a factor m (where m is an integer) and n increased by the same factor; thus such a grating displays multiple higher-order foci of focal length f/m, Figure 2. Similarly, in a linear chirp grating of given structure ($Y_n$) and order of focus, the focal length f varies inversely as $\lambda$, or directly as the optical frequency, as illustrated in Figure 3. This is

usually described as severe chromatic aberration [1], but in principle at least could be exploited to perform optical spectrum analysis, the chirped grating replacing the periodic grating and Fourier Transform lens in a conventional grating spectrometer (although in the present case the spectrum is displayed axially rather than within the focal plane). It is usually desirable to include all possible values of n in a chirped grating (in order to maximise its optical efficiency and peak-to-background illumination levels, as discussed later) but it is not necessary to do so to form a perfect focus as defined above. The simplest example of a 'thinned' grating is one operated at one of the higher order foci discussed above, in which only one in m possible slits is present. A second example would be to choose $L_n = F + n^2\lambda$ which selects just the $0^{th}$, $1^{st}$, $4^{th}$, $9^{th}$..... slits from the full set, and which results in a more nearly periodic grating. Such gratings can be regarded as withdrawal-weighted chirp gratings, the weighting affecting the shape of the focus and its sidelobe structure in the focal plane in a manner reminiscent of weighted optical diffraction gratings [10, 11]. In contrast to conventional lenses, however, we show in section 4 that the behaviour in the axial direction (the x-axis of Figure 1(a)) is of as much interest as that within the focal plane (containing the y-axis in Figure 1(a)). For completeness we add that an alternative weighting procedure, if required, is to vary the slit widths, W.

A grating constructed according to Eq (4) is known as a linear chirp grating because the local spatial frequency, $f_s$, varies linearly with location, Y. Here $f_s$ is the reciprocal of the local slit separation or grating period, $p_n$. From Eq (4) $p_n = \partial Y/\partial n$ so that

$$f_s = \left[\frac{1}{p_n}\right] = \left[\frac{Y}{f\lambda}\right] \tag{5}$$

confirming the linear variation of $f_s$ with Y. This formula is often written as

$$f = \frac{1}{\lambda\left[\frac{\partial f_s}{\partial Y}\right]} \tag{6}$$

In particular, in the discipline of acousto-optics a linearly chirped acoustic waveform can be used (among other things) as a travelling cylindrical lens [6], as shown schematically in Figure 1(b). If V is the velocity of sound and $f'$ the "instantaneous (temporal) frequency" of the electrical waveform driving the acoustic transducer, $Y = Vt$, and $f_s = 1/\lambda_{acoustic} = f'/V$, leading to

$$f = \frac{V^2}{\lambda\left[\frac{\partial f'}{\partial t}\right]} \tag{7}$$

where $\partial f'/\partial t$ is the chirprate. This is the classical formula for the focal length of an acoustic chirp grating[12].

It is clear from Eqs (3) and (4) that the linear chirp grating is only an approximation to an ideal focussing structure. By treating the term $n^2\lambda^2$ in Eq (3) as a perturbation on $2fn\lambda$ it readily shown that for a grating comprising all sources from n = 0 to N the concomitant error in location of the final slit, $\delta Y_N$, as a fraction of the local period, $p_N$, is given by

$$\frac{\delta Y_N}{p_N} = (N.A.)^4 \left[\frac{2f}{\lambda}\right] \tag{8}$$

where the numerical aperture N.A. is defined by

$$N.A. = \frac{D}{2f} \tag{9}$$

D being the aperture of the grating which in the present case is equal to $Y_{max}$. Clearly $\delta Y_N$ exceeds $p_N$ for values of N.A. approaching unity. In these circumstances the constructive interference of the sources leading to the original focus is destroyed, but a degraded focus may reappear elsewhere in the field. From a practical viewpoint gratings of large N.A. are desirable as they produce the highest performance, e.g. as measured by the minimum focal spot width $\Delta \approx \lambda/(2N.A.)$. Small spots are desirable for

example, to access optically stored data as on compact discs. In this connection it is amusing to observe that the smallest attainable focal spot width is determined by the smallest features of the grating, $p_{min}$ or 2W as discussed below. With reference to Figure 1 first note that a slit of width W only radiates significantly over an angular interval $\pm \alpha$ where

$$\alpha \simeq \left[\frac{\lambda}{2W}\right] \qquad (10)$$

so for the finest section of the grating to contribute to the first order focus requires $\theta \simeq \lambda/p_{min} \leq \alpha$, or $W \leq p_{min}/2$. Secondly, the narrowest focal spot obtains if all the slits from $n = 0$ to N are present, when the width $\Delta \simeq \lambda f/Y_{max} \simeq \lambda/\theta \simeq p_{min}$, consequently

$$\Delta \simeq p_{min} \geq 2W \qquad (11)$$

If W is significantly less than $p_{min}/2$, the limiting value $\Delta = 2W$ implied by Eq (11) may be obtained in the higher order foci mentioned earlier as these exploit the full one-sided angular spectrum from 0 to $\alpha$. (In a double-sided grating, i.e. one employing both signs of $Y_n$ in Eq (3), the ultimate spot size is $\simeq W$ since this exploits the two-sided angular spectrum from $-\alpha$ to $+\alpha$. This is illustrated in the Appendix, especially Figure A2). These considerations are obviously pertinant to the fabrication of focussing gratings since they may, for example, necessitate the use of electron-beam lithography to achieve the required feature dimensions and hence focal spot size. In the case of acousto-optics they also have an important consequence for the acoustic frequency, f', while other considerations influence the acoustic delay time, T (or pathlength VT), as discussed below.

An acousto-optic focussing structure is shown schematically in Figure 1b. In this structure the width of the focal spot is given by $w \simeq \lambda f/VT$ where T is the duration of the acoustic wavetrain intercepted by the laser beam (neglecting acoustic attenuation). The preceding discussion shows that the smallest acoustic wavelength should therefore be $\leq w$. If, for example, it is required to make $w \simeq 2\lambda \simeq 1$ $\mu$m, this implies on acoustic response up to at least f' = 5GHz in a typical material with velocity V = 5000 m/s. Other properties of the acousto-optic material of importance are the acoustic propagation loss at the highest frequency, and the acousto-optic figure of merit. In the pulse compression scheme of refs (3) to (5) an important parameter is the compression ratio, C.R. This is the ratio of the waveform duration, T, to that of the compressed spot, $\tau = w/V$. From Eq (7) C.R. is given by

$$C.R. = T^2 \frac{\partial f'}{\partial t} = T.B. \qquad (12)$$

where $B = T\,\partial f'/\partial t$ is the (single-sided) bandwidth of the chirp waveform. Thus the compression ratio equals the *time bandwidth product*, T.B. It is also of interest to note that surface acoustic wave (SAW) techniques are ideal for the production of the required waveforms. For example by impulsing chirped delay lines one may generate a wide range of linear or nonlinear chirp waveforms with or without amplitude weighting [13]. Such waveforms may need to be up-converted, frequency-doubled, etc. to feed the bulk acoustic wave transducer of Figure 1b. In the case of the fixed grating of Figure 1a, the (spatial) compression ratio is the ratio of the illuminated grating aperture D (in the Y-direction) to the width of the focal spot (in the y-direction). It is given by $D^2/(\lambda f)$ which from Eq (6) equals the *space-bandwidth product*, SB,

$$SB = D^2 \frac{\partial f_s}{\partial Y} = D\,\Delta f_s \qquad (13)$$

where $\Delta f_s = D\,\partial f_s/\partial Y$ is the (single-sided) spatial bandwidth of the grating structure, neglecting the harmonic content of the grating structure.

In section 3 the properties of various linear and nonlinear gratings of large N.A. are investigated experimentally and theoretically and compared with each other and with the behaviour of a cylindrical lens. A fascinating variety of second order differences in behaviour is found.

## 3. EXPERIMENTS

In order to investigate the properties of the large N.A. chirp gratings introduced in the previous section we have constructed 4 test patterns. These each had a (first-order) focal length of 1cm and were designed for operation at $\lambda = 0.5145\mu m$. Two of the gratings contained 350 slits (n = 0 to 349) and were of the ideal nonlinear design Eq (3), and linear design, Eq (4), respectively. In each case $Y_{max} \simeq 1900\mu m$, giving numerical apertures N.A. $\simeq 0.1$, Eq (9). The other two patterns were similar but omitted the first 150 slits, so covered the range n = 150 to 349. These patterns occupied the range $Y \simeq 1240$ to $1900\mu m$ and so had an N.A. $\simeq 0.033$. The finest spatial period of each grating was $p_{min} \simeq 2.8\mu m$, and to satisfy the conditions outlined in section 2 , the slit width was made $W \simeq 1.4\ \mu m$ throughout each grating. This width is sufficiently large ($W \simeq 3\lambda$) that it avoids the polarization-dependent complications of very fine structures [14], at least as far as the first order focus is concerned. The devices were constructed on high resolution chrome photo-plates which had an optical density of $\simeq 3$.

The measured behaviour of these gratings in the vicinity of their 1st order foci has been compared with calculations based on scalar diffraction theory and the results are presented in Figure 4(a) to (d). In each case the agreement between measurement and calculation is good, minor improvements to the theory would arise by inclusion of the sinc-function radiation patterns from the individual slits due to the finite value of W, and the $r^{-1/2}$ variation of the amplitude away from each slit (line source). We now comment on the detailed behaviour of each grating response in turn.

Figure 4(a) shows the response of the 200-slit ($n \simeq 150 - 349$) grating with the ideal non-linear chirp structure of Eq (3). The focus occurs at the designed point and the response in the focal 'plane' ($x = f$) is very nearly of sinc-function form, with the correct width to within about 6%, Figures 5(a) and (b). This behaviour is almost identical to that of the corresponding section of a cylindrical lens.

Figure 4(b) shows the response of the corresponding linear chirp grating in which the slit locations were derived from Eq (4). The principal difference from (a) is the shift in the focus towards the grating by $\simeq 360\mu m$, and the accompanying small vertical shift $\Delta y \simeq 40\mu m$. The origin of this phenomenon is readily appreciated when it is recalled that the linear chirp of Eq (4) was derived from the ideal nonlinear chirp formula of Eq (3) by dropping the term $n^2\lambda^2$. Thus the patterns match for small n and progressively diverge for larger n. In the present case (n = 150 - 349) all the slits of the linear chirp grating are displaced to smaller y-values resulting in higher spatial frequencies and a greater chirp rate. To compute the location of the new focus we should find that nonlinear chirp pattern which is a best approximation to the linear chirp pattern over its span, e.g. by matching the periods and chirprates at the (effective) centre of the grating. Carrying out this process leads to the following formulae for the focal displacement of the linear chirp grating

$$\Delta x \simeq -3c\lambda$$
$$\Delta y \simeq +(2c\lambda)^{3/2}\ f^{-1/2} \qquad (14)$$

where c is the number of the central slit. Taking c as the numerically central slit for the present grating ($n = 150 - 349$, $c = 250$) predicts $\Delta x = -386\mu m$ and $\Delta y = +41\mu m$, which values compare quite well with the measured and numerically calculated fields in Figure 4(b). For this device the peak intensity at the new focus is not quite as high as in Figure 4(a) because the wavelets from the slits are nowhere perfectly in phase. Nevertheless a reasonably well-defined focus remains. In this context it is interesting to note the shift of the focus in the *y-direction*. This degree of freedom is not available to a double-sided linear chirp grating (or to a zone plate lens) since the 'focus' is constrained to lie on the x-axis by symmetry. Consequently 2-sided gratings show a poorer but symmetrical focus, which is the (complex) superposition of ? fields, e.g. that of Figure 4(b) and its mirror image in the x-axis. This is discussed in more detail in the Appendix.

Turning now to the chirp gratings containing 350 slits (n = 0 - 349), first consider the nonlinear version (derived from Eq (3)), whose measured and calculated responses are

shown in Figure 4(c). The focus is unshifted from the design point and on the linear intensity scale shown is superficially 'perfect'. However detailed examination on a logarithmic (dB) scale reveals some interesting departures from the (almost) sinc-function form of Figure 4(a). These differences are shown in detail in Figures 5(c) and (d). Firstly the -3dB width is increased by ~20% over that of the ideal sinc-function form for the same aperture, $Y_{max}$. Secondly the close-in sidelobe structure is largely washed out. A third feature which is not shown in Figure 5 is that the overall response is not quite symmetrical in y; the same was actually true of Figure 4(a), but to a minute degree. The physical explanation of this effect is straightforward. If we compare the grating shown schematically in Figure 1 with half of a cylindrical lens it is immediately apparent that the grating is weighted in favour of the high spatial frequency end as a result of the greater density of sources there. This variable density of slits had a very small effect in the case of the 200-slit gratings of Figure 4(a) and (b) because they omitted the low-n section of the gratings where the density varies most rapidly. In the case of gratings extending from n = 0 to N it is shown in the Appendix that, if required, the sinc-function behaviour of a cylindrical lens can largely be restored by weighting the slit strengths in inverse proportion to the local period so as to recreate a quasi-uniform overall intensity transmission through the grating. This could most easily be achieved in practice by employing a 1:1 mark/space ratio, as in the case of zone-plate lenses or by using the withdrawal-weighting scheme discussed in section 2. However, there are two reasons to question the usefulness of such a procedure. Firstly the sidelobe suppression may well be desirable in its own right; for example in the case of pulse compression radar it is normal practice to deliberately build such suppression into the compressor to avoid the appearance of false targets [15]. Secondly, the field in the focal plane of chirp gratings (and zone-plate lenses) is complicated by "spurious" radiation from the higher grating orders responsible for the higher order foci mentioned earlier, and from the zero-order. The latter is direct transmission through the grating which may be regarded as producing a zeroth-order focus at infinity (x = f/0). In particular, this zero-order radiation interferes strongly with the close-in sidelobes of gratings containing slits of small n-value such as our 350-slit devices. This effect is illustrated in Figure 6. Roughly speaking the ratio of the intensity at the focus to the average background level is N, the number of slits, since the amplitudes add constructively at the focus and more-or-less randomly elsewhere. However the background intensity close to the focus is reduced from the average value precisely because of the paucity of slits for small values of Y in Figure 1a. Increasing the intensity of these sources raises the background level in the vicinity of the focus and washes out the sidelobes! Indeed to avoid this interference altogether it is desirable to omit the low-n sources, as in our 200-slit patterns, but this is at the expense of a wider focal spot.

The final device to be considered is the 350-slit linear chirp device of Figure 4(d). The principal features of this are the elongated and curved "focus" which arises because different sections of the grating focus at different points, Eq (14). This distribution of focal points from different sections of the grating also accounts for the asymmetric "sidelobe" distribution in Figure 4(d) and is reminiscent of (and related to) the caustic cusp seen in a teacup. In the present work this distributed focus is an unwanted feature of a linear chirp grating, which can be eliminated by using an ideal nonlinear grating pattern. However, in a recent publication Frère and Bryngdahl have shown that this phenomenon can be *exploited* to generate 3-D curves of continuous foci in space [16].

## 4. AXIAL MEASUREMENTS

The discussion to date has concentrated on the field in the focal plane, which we have compared to that of a cylindrical lens. In some applications of chirp gratings such a variation is the relevant one e.g. in the travelling lens [6] and acousto-optic pulse compression scheme [3-5]. There are, however, several reasons for additionally investigating the response along the axis y = 0 in Figure 1. One such reason is that the higher order foci occur axially rather than in the focal plane, as they do in a

conventional grating spectrometer. A second reason concerns the frequency (or wavelength) response at the focus. In a conventional grating spectrometer this is of sinc-function form and mimicks the spatial response at fixed wavelength. In the present device it is clear that (in the limit $W \to 0$) the impulse response h(t) at the first-order focus comprises N $\delta$-functions of constant incremental delay $\delta t = \lambda/c$ where c is the velocity of light. The frequency response, H(f), is the Fourier Transform of h(t) and is therefore of sinc-function form, in contrast to the spatial response in the y-direction of Figures 5(c) and (d). It is shown below that in chirp gratings this sinc-function frequency response mimicks the spatial response in the *axial* direction.

Figure 7 illustrates the construction used to calculate the response in the region of the focus, for small deviations in the x and y directions. Assuming an ideal nonlinear chirp grating constructed according to Eq (3) we have from Figure 7(a),

$$M_n^2 = L_n^2 + 2fx + x^2 \tag{15}$$

$$M_n \simeq L_n + x - \left[\frac{n\lambda x}{f}\right] + \ldots\ldots\ldots \tag{16}$$

Since all the sources add constructively at the focus, F, the amplitude at a distance x from F is given by

$$a(x) \propto \sum_n \exp -jk(M_n - L_n) \tag{17}$$

$$\propto \exp -jkx \sum_n \exp +j\left[\frac{2\pi nx}{f}\right] \tag{18}$$

Apart from the premultiplying linear phase-factor the summation in Eq (18) is of the same form as that for a conventional diffraction grating and the response is therefore of sinc-function form. For a grating comprising M slits the intensity, I, varies as

$$I(x) \propto |a(x)|^2 \propto \frac{\sin^2 [M\pi x/f]}{\sin^2 [\pi x/f]} \tag{19}$$

The depth of focus, $\delta$, measured along the x-axis can be calculated from Eq (18) by invoking Rayleigh's criterion, which states that one remains sensibly in focus providing the total spread in phases does not exceed $\pi/2$. This gives

$$\delta = \pm\left[\frac{f}{4M}\right] \tag{20}$$

the intensity dropping to ~ 80% of its peak value at $x = \pm\delta$. In the case of gratings extending from n = 0 to N, Eq (20) may be written

$$\delta = \pm\left[\frac{\lambda}{8\ N.A.^2}\right] \tag{21}$$

It is clear from Eq (19) that the response in the x-direction now mimicks the sinc-function frequency response, H (f), deduced earlier from the impulse response. Indeed the frequency response could otherwise be derived by letting the wavevector k in Eqs (17) and (18) relate to a variable wavelength, $\lambda'$, when the response evidently becomes a function of the product $k'x$. This is reminiscent of a conventional diffraction grating in which the response is a function of the product $k \sin\theta$.

It is also interesting to observe the close resemblance between Eq (18) and the Fourier Transform relationship. This may be extended by generalizing the discussion to allow variable slit source strengths, $b_n$, when the modulus of the amplitude a(x) is given by

$$|a(x)| \simeq \left| \sum_n b_n \exp +j\left[\frac{2\pi nx}{f}\right] \right| \tag{22}$$

If, for example, the $b_n$ uniformly sample a slowly-varying function, b, at the Nyquist

rate or faster, then the sampling theorem ensures that the $|a(x)|$ will reproduce the modulus of the Fourier Transform of b. Similarly an appropriately sampled version of $|a(x)|$ may be regarded as the modulus of the discrete Fourier Transform of the $b_n$. Turning now to the y-dependence of the field in the region of the focus, we have from Figure 7(b)

$$Q_n^2 = f^2 + (Y_n - y)^2 \tag{23}$$

$$= L_n^2 - 2Y_n y + y^2 \tag{24}$$

whence

$$Q_n - L_n \simeq \left[\frac{y^2 - 2Y_n y}{2L_n}\right] + \ldots\ldots\ldots \tag{25}$$

$$\simeq \left[\frac{y^2}{2f}\right] - y\left[\frac{2n\lambda}{f}\right]^{\frac{1}{2}} + \ldots\ldots\ldots \tag{26}$$

The field amplitude is therefore given by

$$a(y) \simeq \sum_n \exp -jk(Q_n - L_n)$$

$$\simeq \exp -\left[\frac{jky^2}{2f}\right] \sum_n \exp +jky\left[\frac{2n\lambda}{f}\right]^{\frac{1}{2}} \tag{27}$$

This expression contains an unimportant premultiplying nonlinear phase factor and a summation in which the exponents vary directly as y, but as $n^{\frac{1}{2}}$. The Fourier Transform-like relationships just discussed are therefore modified, so that a sinc-function variation should not be expected in the y-direction. Nevertheless the amplitude peaks at $y = 0$, and on physical grounds may be expected to decline significantly when the net phase shift from the first to last source amounts to $2\pi$ [17]; some appropriate phasor diagrams are illustrated in Figure 8 for a nonlinear chirp grating with $n = 0$ to 349. From this discussion and Eq (27) we expect the FWHM to be of order $\delta y$ where

$$k\,\delta y\left[\frac{2N\lambda}{f}\right]^{\frac{1}{2}} \simeq 2\pi \tag{28}$$

leading to

$$\delta y \simeq \left[\frac{f\lambda}{2N}\right]^{\frac{1}{2}} \simeq \left[\frac{\lambda f}{Y_{max}}\right] \tag{29}$$

This approximate relationship happens to be identical to the classical value expected for a numerical aperture N.A. = $Y_{max}/2f$, Eq 9. However, as noted earlier the measured and calculated FWHM of our 350-slit nonlinear chirp grating is actually 20% greater than the classical value, see Figure 4c.

In the case of a grating containing a small number of sources centred on $n_c >> 1$, the square root in Eq (27) may be expanded as follows. If $n = n_c + \Delta n$

$$n^{\frac{1}{2}} \simeq n_c^{\frac{1}{2}}\left[1 + \frac{\Delta n}{2n_c}\right] \tag{30}$$

In these circumstances Eq (27) becomes

$$a(y) \simeq \exp -\left[\frac{jky^2}{2f}\right] \exp +jky\left[\frac{2n_c\lambda}{f}\right]^{\frac{1}{2}} \sum_{\Delta n} \exp +jky\Delta n\left[\frac{\lambda}{2n_c f}\right]^{\frac{1}{2}} \tag{31}$$

Apart from the premultiplying nonlinear phase factor, this has restored the sinc-function form of a(y), the first zeros occurring when

$$ky\Delta n\left[\frac{\lambda}{2n_c f}\right]^{\frac{1}{2}} = \pm 2\pi \qquad (32)$$

or $$y = \pm\left[\frac{\lambda f}{D}\right] \qquad (33)$$

where the aperture $D = f\Delta n(\lambda/2fn_c)^{\frac{1}{2}}$ in the present approximation. This description is reasonably valid for the 200-slit nonlinear chirp grating of Figures 4(a) and 5(a), whose behaviour is of course extremely similar to that of an appropriate section of a cylindrical convex lens.

## 5. FAR-FIELD MEASUREMENTS

Almost all interest in chirp gratings to date has concentrated on their focussing properties in the near/intermediate field, Figure 1. However chirp gratings are one particular example of the class of weighted diffraction gratings discussed in refs (10) and (11), and it is therefore of some interest to consider their response in the far-field. It is well-known that the Fraunhofer or far-field distribution is closely related to the Fourier Transform of the field at the exit plane of the grating, which is of course a replica of the grating structure itself. Thus the measured far-field intensity patterns in the ±1 orders of Figure 9, confirm the anticipated quasi-rectangular frequency spectrum of a linear chirp waveform [15]. They are in fact measures of the spectra of the spatial frequencies, $f_s$, or temporal frequencies, $f'$, of section 2. Note, however, that because the detector is only sensitive to intensity, the dispersive phase response of the chirp waveform is lost in these measurements. The response of acousto-optic devices in the far-field is of course exploited in the acousto-optic spectrum analyser [18]. Interest in the far-field response of static chirped gratings could arise from the flatness of the response and low sidelobe levels attainable with the optimum weighting.

## 6. CONCLUSION AND DISCUSSION

In this paper the basic properties of (static) one-dimensional focussing chirp gratings have been reviewed, and the discussion extended to incorporate some related properties of *travelling* acoustic chirp waveforms. It has been emphasized that the commonly discussed linear chirp structure is only an approximation to the ideal nonlinear form, a consideration that becomes increasingly important in high-performance components employing large numerical apertures. The measurements of section 3 confirmed the calculated behaviour of such devices in numerous respects including the shifts in the location of the best focus, and the distortion of the focal spot from the ideal sinc-function form. The discussion in section 4 revealed the significance of the axial variation of the field near the focus, showing for example that it is this axial variation that mimicks the frequency response obtaining at the focus. This contrasts with a conventional grating spectrometer where the frequency response mimicks the spatial response in the focal plane. It is also interesting to observe that, in contrast to the focal plane response in Figure 6, the axial response is relatively unaffected by the 'spurious' radiation into the higher grating orders, especially if the low-n sources are absent.

While the discussion has concentrated on the first-order diffraction from the grating (leading to the formation of the first-order focus) mention has often been made of the presence of the zero-order and higher diffraction orders and foci. For example it has been shown that some of the spurious features in the first-order focal plane can be interpretted as arising from "pinhole camera images" of the grating as imaged through the individual higher order foci. It is also of interest to note that the consequences of using a non-ideal chirp grating become more severe at the higher order foci. In fact the ideal nonlinear chirp design discussed in section 2 is only ideal at one chosen focus (the first-order focus in the devices of section 3) and so the higher order foci are displaced and severely degraded for both the linear and nonlinear designs studied in

section 3. This point is graphically illustrated by considering two neighbouring slits separated by the local period, $p_n$. These sources are unable to contribute constructively to an $m^{th}$-order focus *anywhere in the field* if $p_n < m\lambda$. Consequently the contribution from the high-n sources to the higher order foci declines progressively with increasing order. This aspect is not discussed in detail here, however, as the behaviour is further complicated by a progressive decline in the contributions from the high-n sources as a result of the finite slitwidth, W. Indeed, (in contrast to the first order foci) we have found it necessary to include in our calculations the finite slitwidth in order to account for the measured positions of the $2^{nd}$-order foci. Additionally an interesting observation has been made on the second-order foci of the gratings of section 3 in which the contribution from the highest-n slits should vanish according to scalar diffraction theory since $W = p/2$ . In these devices we observed that the detailed structure of the focus was dependent on the polarization of the input light beam; vector diffraction theory is evidently necessary to explain such observations [14].
Finally we comment on the optical efficiency of the gratings used in this work. This is inherently low (at most a few percent) due to the loss of light in the opaque regions of the mask and the scattering into unwanted diffraction orders, principally the zeroth. The former loss would obviously be increased if the gratings were withdrawal-weighted in the manner discussed earlier, so it is desirable to retain as many slits as possible in a practical design. Concerning the loss of light into unwanted orders, as in the case of zone plate lenses this loss can be educed by replacing (at least some of) the opaque region of the mask with $\lambda/2$ dielectric layers, to form the analogue of a phase reversal zone plate [1].

ACKNOWLEDGEMENT

It is a pleasure to acknowledge the skill of George Gibbons in producing the gratings.

REFERENCES


1. HECHT, E. and ZAJAC, A. : 'OPTICS', Addison-Wesley, 1974, Ch.10.

2. LEITH, E. N. : 'Synthetic Aperture Radar', Topics in Applied Physics 23, OPTICAL DATA PROCESSING, Ed. D.Casasent, Springer-Verlag, 1978, Ch.4.

3. GERIG, J. S. and MONTAGUE, H. : 'A Simple Optical Filter For Chirp Radar', Proc. IEEE, 52, 1964, p.1753.

4. SCHULZ, M. B., HOLLAND, M. G., and DAVIS, L. : 'Optical Pulse Compression Using Bragg Scattering By Ultrasonic Waves', App. Phys. Lett., 11, 1967, pp237-240.

5. COLLINS, J. H., LEAN, E. G. H., and SHAW, H. J. : 'Pulse Compression by Bragg Diffraction of Light with Microwave Sound', ibid pp240-242.

6. MERRY, J. B., and BADEMIAN, L. : 'Acousto-optic Laser Scanning', Proc. SPIE, 169, 1979, pp56-59.

7. YAO, S. K., FINDAKLY, T., FOROUHAR, S., WARREN, C., and CHANG, W. S. C. : 'The State Of Art Of Chirp Grating Lenses On $LiNbO_3$', Proc. SPIE 408, 1983, pp90-94.

8. BARNARD, M. E., LANCASTER, M. J. and PAIGE, E. G. S. : 'A Novel Spectrum Analyser Based On The Slanted Chirped Transducer', Proc. 1984 IEEE Ultrasonics Symposium pp103-107.

9. BARNARD, M. E., LANCASTER, M. J. and PAIGE, E. G. S. : 'A Theoretical Investigation of the Focussing of the SCT' ibid 1985 pp32-37

10. LEWIS, M. F. and WEST, C. L. : 'Weighted Optical Diffraction Gratings', to be published in Applied Optics, June 1988.

11. LEWIS, M. F. and WEST, C. L. : 'A Theoretical and Experimental Investigation into the use of SAW Weighting Techniques in Optical Diffraction Gratings' RSRE Memorandum 4128 (1988)

12. KORPEL, A. : 'Acousto-optics. A Review of Fundamentals' Proc. IEEE 69 (1981) pp48-53

13. MAINES, J. D. and PAIGE, E. G. S. : 'Surface Acoustic Wave Devices for Signal Processing Applications' Proc. IEEE 64 (1976) pp639-652

14. PETIT, R. (Ed) : "Electromagnetic Theory of Gratings" Topics in Current Physics 22 Springer-Verlag 1980

15. KLAUDER, J. R., PRICE, A. C., DARLINGTON, S. and ALBENSHEIM, W. J. : 'The Theory and Design of Chirp Radars' B.S.T.J. Vol.39 pp.745-808 July 1960.

16. FRERE, C. and BRYNGDAHL, O. : 'Computer-generated Holograms: Reconstruction of Curves in 3-D' Optics Communications Vol.60, No.6, pp.369-372, December 1986.


17. Note that this criterion is closely related to Rayleigh's criterion. According to Rayleigh the net amplitude is little affected if the range of phases is less than $\pi/2$. Conversely, it is significantly affected if the range of phases exceeds $2\pi$, since then some sources necessarily cancel others.

18. BERG, N. J. and LEE, J. N. (Eds) : 'Acousto-optic Signal Processing' Marcel Dekker Inc., 1983.

Appendix 1

The purpose of this appendix is to discuss in more detail two aspects of focussing chirp gratings which were only briefly mentioned in the text. These concern (i) double-sided gratings, and (ii) the consequences of weighting both single-sided and double-sided nonlinear chirp gratings to restore a sinc-function behaviour in the y-direction of the output plane. The results presented below all derive from calculations based on scalar diffraction theory, and it may be noted that no experiments were performed to verify the calculated behaviour. However, the good agreement between calculation and experiments in Figures 4 and 5 of the main text gives confidence in the results calculated below. In order to illustrate all the effects 'cleanly', we have chosen to base all the calculations on chirp gratings containing 275 slits rather than 350 slits as used in the main text. Thus the single-sided gratings comprise slits n = 0 to 274. The double-sided gratings simulated below comprise 549 slits, viz n = -274 to + 274. Figure A1 compares the behaviour in the region of the first-order focus of four chirp grating designs :-

(a) A 1-sided nonlinear chirp grating containing 275 slits (n = 0 to 274). The behaviour is similar to that in Fig 4c, showing a 'perfect' focus at ($\Delta x = 0$, $\Delta y = 0$).

(b) A 1-sided linear chirp grating containing 275 slits (n = 0 to 274). The behaviour is similar to that in Fig 4d showing a slightly degraded focus with x-offset, $\Delta x \simeq -200\mu m$, and y-offset $\Delta y \simeq +16\mu m$.

(c) A 2-sided nonlinear chirp grating containing 549 (= 2x275-1) slits. This shows a 'perfect' focus at ($\Delta x = 0$, $\Delta y = 0$), and is essentially the superposition of two plots (a) above, i.e. the original and its mirror image in the axis y = 0. The interference between these two (complex) fields is only significant near this axis, and the narrowness of the resulting focus relative to (a) alone is commented on below in connection with Figure A2.

(d) A 2-sided linear chirp grating containing 549 (= 2x275-1) slits. This shows a very degraded focus (at $\Delta x \simeq -60\mu m$, $\Delta y = 0$) and is essentially the superposition of two plots (b) above. For devices with more slits, the focus on axis ($\Delta y = 0$) is even more severely degraded, the best remaining foci being those of the individual 1-sided chirp gratings, as in (b) above.

In Figure A2 (a) and (c) we show in more detail the fields in the focal 'plane' ($\Delta x = 0$) of the nonlinear chirp devices of Fig A1(a) and (c) respectively. These fields are plotted on an optical dB scale to illustrate the various points of interest. In addition, Figs A2(b) and (d) show the corresponding fields for nonlinear chirp gratings weighted in such a manner as to eliminate the effects of the variable density of slits as a function of Y. Thus for example the slit n = 0 is given the largest weight because the local period, p, is greatest at n = 0. This weighting procedure ensures that a uniform average intensity emerges from the grating (roughly resembling that transmitted through a cylindrical convex lens) and so results in a closely sinc-function field in the focal plane. No results are presented for *linear* chirp gratings because the foci are already degraded to some extent by the departure from ideal nonlinearity, and the location of the 'best' focal plane is somewhat uncertain. We now comment on the individual plots of Figure A2 in turn.

(a) This illustrates the perfect focus (0dB loss) of a 1-sided nonlinear chirp grating, and is similar to fig 5(d), showing 'washed out' sidelobes. The full width at the -4dB points is $4.08\mu m$, i.e. somewhat greater than $\lambda f/D \simeq 3.05\mu m$. This arises because of the effective weighting due to the variable density of slits in the Y-direction.

(b) This illustrates the calculated behaviour of a similar grating to (a), but in which the slits are weighted in inverse proportion to the local period, p. This has restored an

almost sinc-function field in the focal 'plane', $\Delta x = 0$. The full width at the -4dB points is 3.12$\mu$m, and extremely close to $\lambda f/D \simeq 3.05\mu$m.

(c) This illustrates the field in the focal plane of a 2-sided nonlinear chirp grating. For direct comparision with (a) above the $\Delta y$ coverage (-10 to +10$\mu$m) has been halved, since the focal width should be halved in a device of double aperture. The focus is perfect (0dB loss) at ($\Delta x = 0$, $\Delta y = 0$) but is narrower than expected for the grating aperture according to the classical formula $\lambda f/D$, and the close-in sidelobes are much stronger than those of a sinc-function. The calculated full width at the -4dB point is 1.28$\mu$m, compared to $\lambda f/D \simeq 1.53\mu$m. The cause of this behaviour is the effective weighting of the grating caused by the variable density of slits in the Y-direction. It is important to note that, in contrast to the 1-sided gratings discussed above, this effective weighting reduces the strength of the centre of the overall grating structure rather than one side. This accounts for the narrowing of the central lobe and the increased sidelobe levels as can readily be seen by considering the limiting case of very strong weighting. With very strong weighting only the outermost sources of the grating would be effective, leading to an approximately cosinusoidal pattern, similar to that arising from Young's slits. This illustrates the origin of the high sidelobe levels. In addition it will be recalled that the central fringe of a Young's slit pattern is only half as wide as that of a single slit whose width equals the separation of the two Young's slits. This is the physical explanation of the narrowing observed in Figure A2(c). This behaviour is also readily visualised if the responses are calculated using the familiar phasor summation procedures.

(d) This illustrates that a sinc-function response is restored to pattern (c) above if the source strengths are weighted in inverse proportion to the local grating period, p. In fact this calculated response is very close to sinc-function form and almost identical to that of (b) above, apart from the scaling by a factor of 2 due to the change in overall aperture from the 1-sided to 2-sided gratings.

An interesting point to emerge from Figure A2 is that the weighting arising from the variable slit density of chirp gratings (a) broadens, and washes out the sidelobes of 1-sided gratings, but (b) narrows, and increases the sidelobes of 2-sided gratings.

FIGURE 1.

(a) Schematic representation of the chirped optical diffraction grating. The slits in the grating are of width W and have Y-coordinates defined by Eqs (3) and (4) in the text. The first order focus occurs at F and is chosen to be in-line with the zeroth slit position. This behaviour is similar to that of one half of a cylindrical lens.
(b) Schematic of a focussing grating formed by a linearly chirped acoustic waveform in a Bragg cell. The acoustic column is launched from the transducer at the bottom of the cell and focusses collimated light at F. As the acoustic wave propagates across the cell the focal spot translates across the focal plane at the velocity of sound, V, (in the acoustic medium). In this configuration it is necessary to reduce the transducer width to satisfy the Bragg reflection conditions approximately for all the rays; in the optimum configuration there is only strong coupling to the $1^{st}$ diffraction order and, in principle, diffraction efficiencies approaching 100% can be realised. For simplicity the complications of the refractive index of the acoustic medium are omitted.

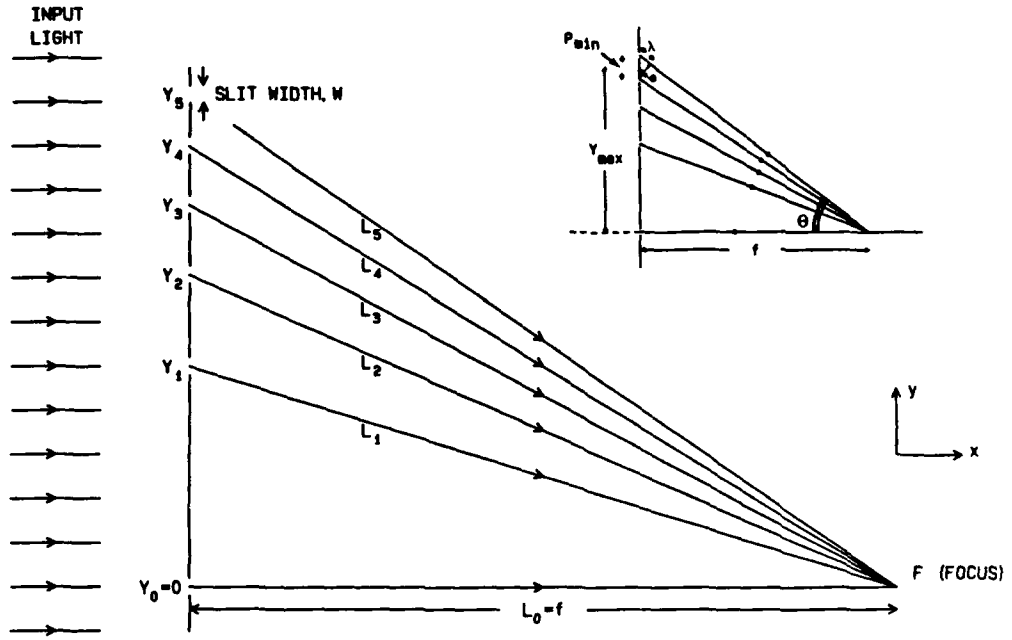


FIGURE 1a

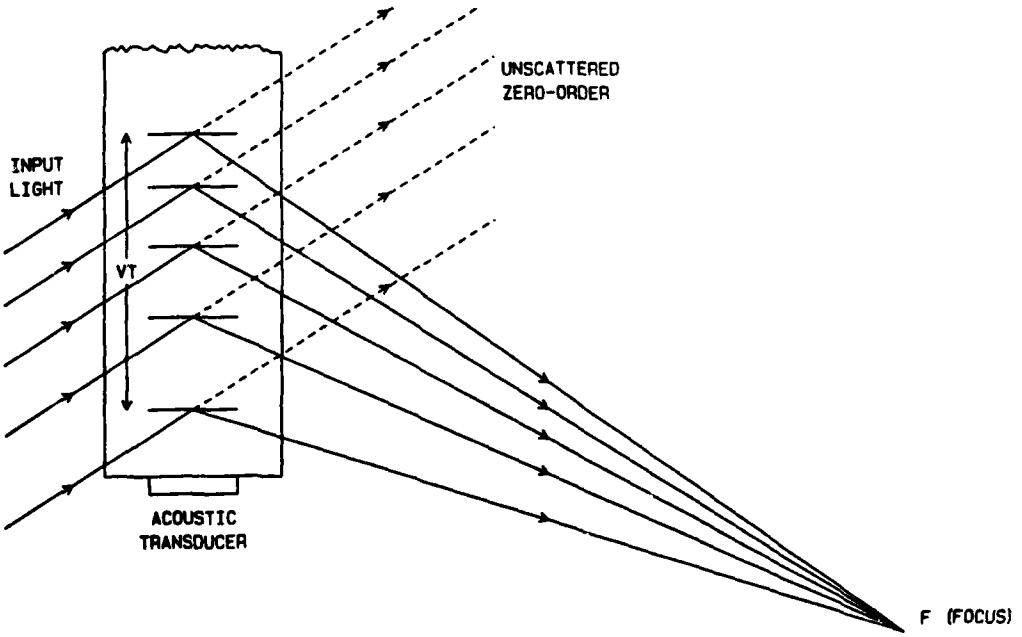


FIGURE 1b

FIGURE 2.

Multiple exposure displaying the zero-order transmission and the formation of the first and higher order foci of a 350-slit nonlinear chirp grating. This composite photograph of the field in the (x,y) plane was obtained by rotating the grating mask through 45° about the Y-axis in Figure 1a, and taking a series of photographs obtained using a T.V. camera with its plane perpendicular to the x-axis in Figure 1a. This camera employed auto-gain and gamma correction to eliminate intensity variations across the field. The grating itself also appears in the figure, the individual slits of low-n value being well resolved. As discussed in the text the second order focus is narrower than the first order focus due to its higher N.A. In the 200-slit gratings the higher order foci are much weaker than in the 350-slit patterns due to the absence of the low-n sources, again as discussed in the text.

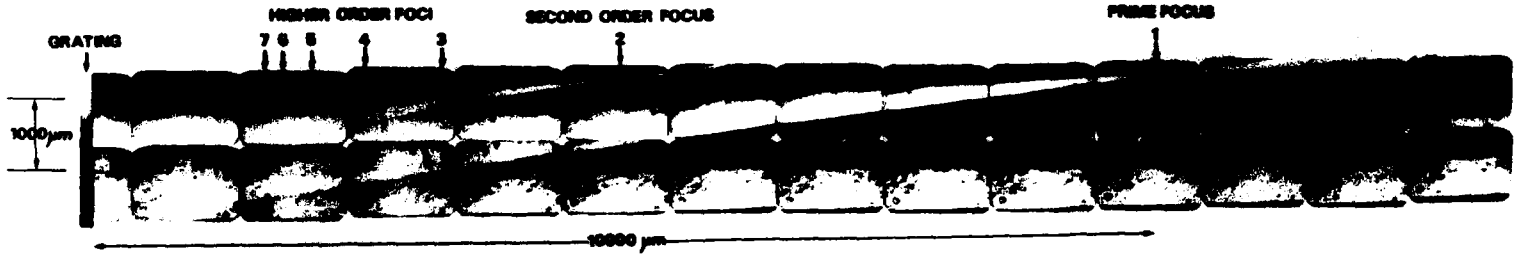


**CHIRP GRATING : 350 SLITS : NON-LINEAR**

FIGURE 2

FIGURE 3.

Response of the 350-slit nonlinear chirp diffraction grating to a multi-line illumination from an Argon Ion laser. The grating was designed for operation at 514.5nm and the figure demonstrates the axial displacement of the foci at various shorter wavelengths. The arrows show the calculated positions of the foci. In these and certain other measurements precautions were taken to avoid spurii caused by multiple reflections in the mask plate.

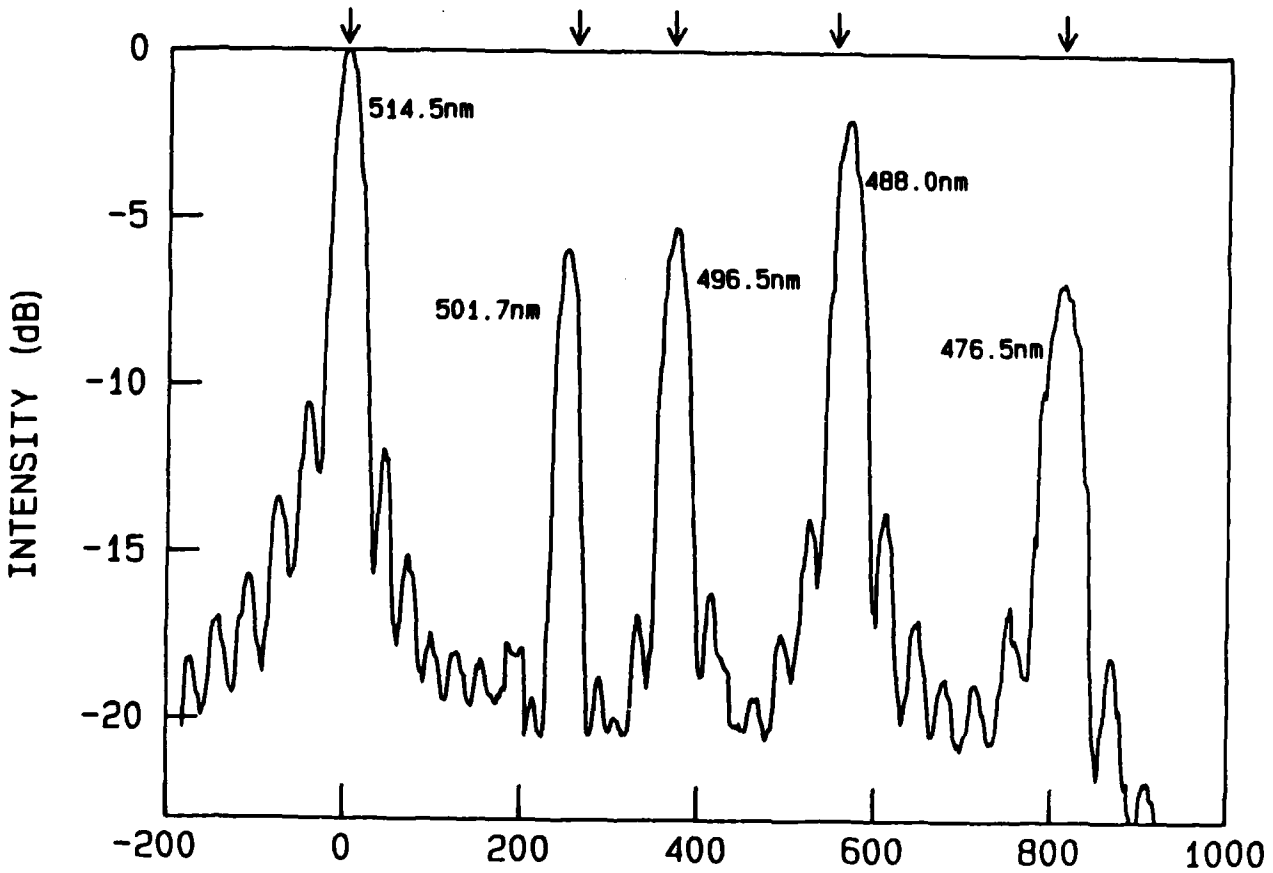
0
-5
-10
-15
-20
INTENSITY (dB)
514.5nm
501.7nm
496.5nm
488.0nm
476.5nm
-200
0
200
400
600
800
1000
x-DISPLACEMENT (microns)

FIGURE 3

FIGURE 4.

The behaviour of the chirped diffraction gratings in the vicinity of their first order foci. The focussing action is illustrated in perspective by adding a linear measure of the optical intensity to the x-coordinate.
a) 200-slit nonlinear chirp grating (Eq (3), n = 150 to 349)
b) 200-slit linear chirp grating (Eq (4), n = 150 to 349)
c) 350-slit nonlinear chirp grating (Eq (3), n = 0 to 349)
d) 350-slit linear chirp grating (Eq (4), n = 0 to 349)
The left hand figure of each set displays the calculated responses (omitting the element factor for the slit width), which are evidently in good agreement with the measured responses on the right. Notice the displacement of the foci in (b) and (d) which from Eq 14 are calculated to be ($\Delta x = -386\mu m$, $\Delta y = +41\mu m$) and ($\Delta x = -270\mu m$, $\Delta y = +24\mu m$) respectively. .
Concerning the depth of focus, the conventional measure would be along the x-direction, the symmetry axis of Eq (3). Clearly for our one-sided gratings the depth of focus is greater if one measures along an inclined axis. Notice that in (d) this axis is curved due to spherical aberration.

FIGURE 4a 200-SLIT NONLINEAR CHIRP GRATING

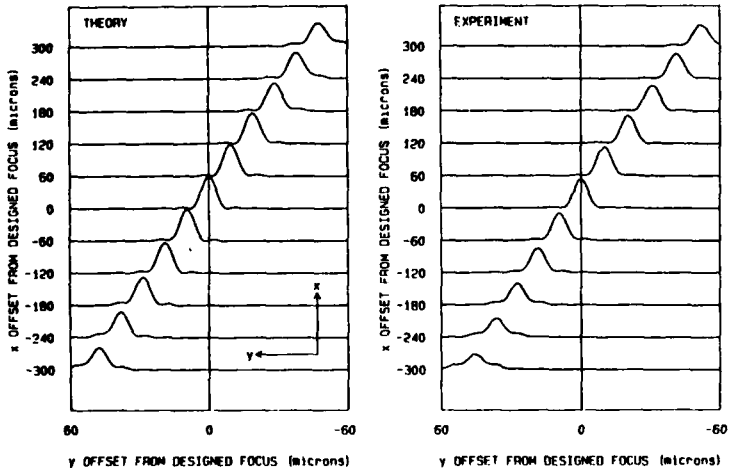


FIGURE 4b 200-SLIT LINEAR CHIRP GRATING

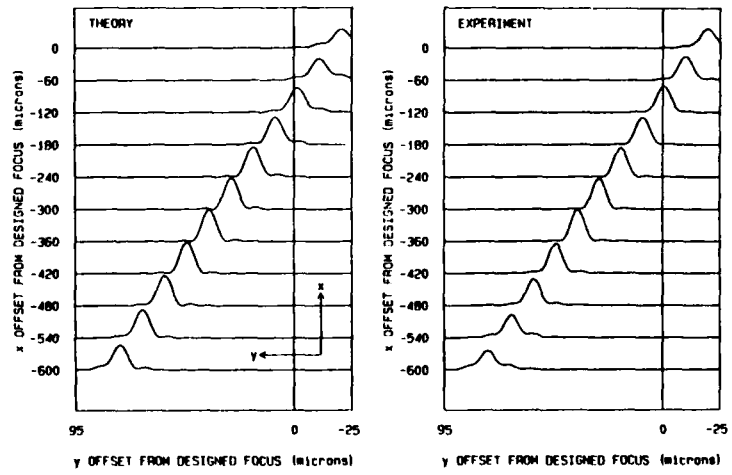


FIGURE 4c 350-SLIT NONLINEAR CHIRP GRATING

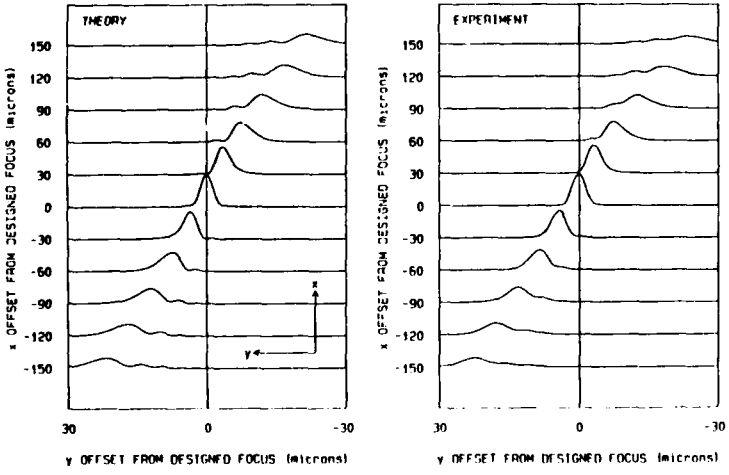


FIGURE 4d 350-SLIT LINEAR CHIRP GRATING

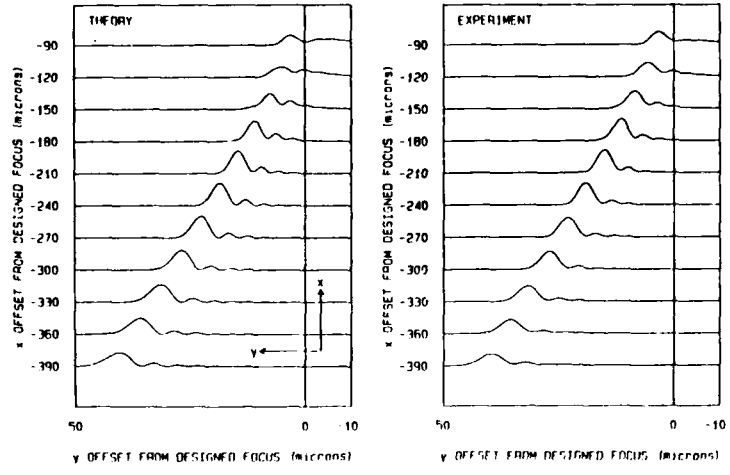

FIGURE 5.

Experimental and theoretical responses of the nonlinear chirped gratings in the vicinity of the first order focus on a logarithmic intensity scale. (a) and (b): For the 200-slit grating the response is almost of sinc-function form in both directions. (c) and (d): For the 350-slit grating the intensity shows a sinc-function form along the x-direction, while in the orthogonal direction the nulls are suppressed as explained in the text. For this measurement it was critical to align the focus and the zeroth slit position accurately to define the x-axis, as a minor angular offset compresses or expands the scale significantly as is clear from the depth of focus considerations in the caption to Figure 4. The linearly chirped gratings have displaced and extended foci, and so it is not possible to produce equivalent meaningful comparison plots for these cases.

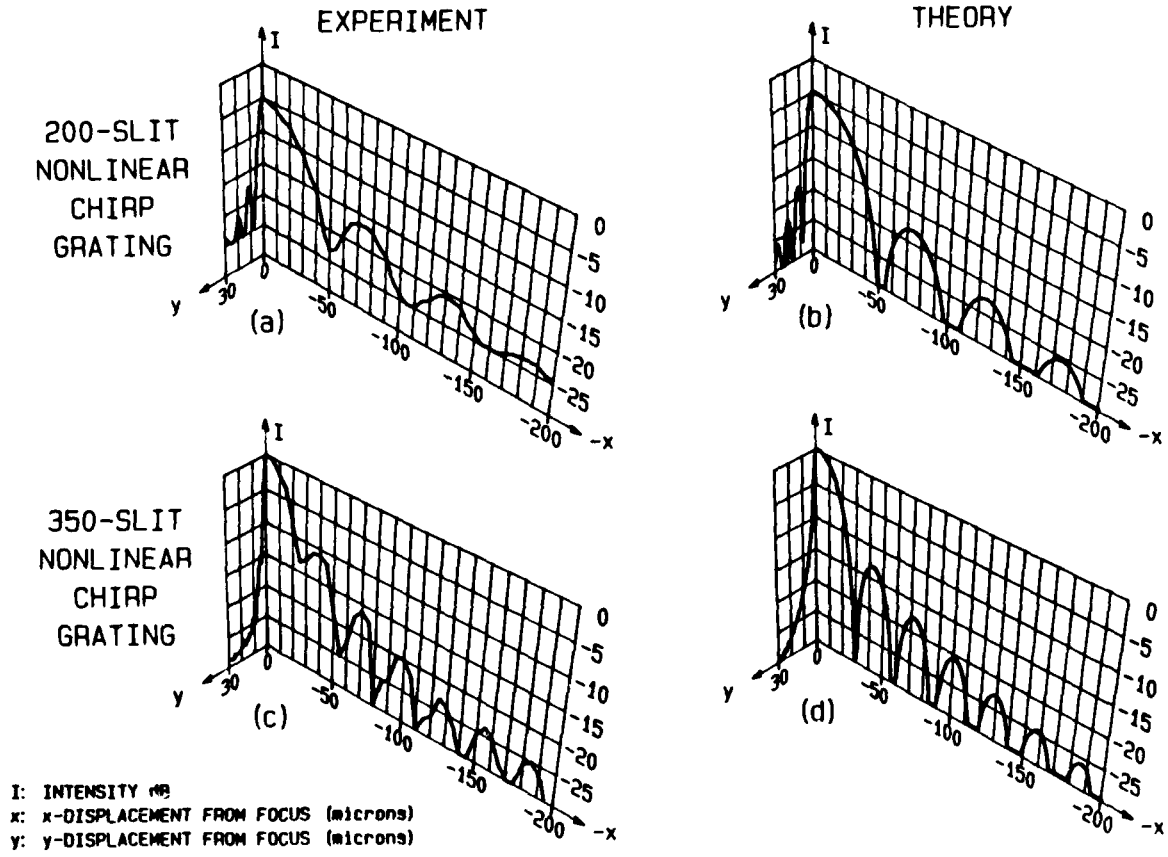
EXPERIMENT
THEORY
200-SLIT
NONLINEAR
CHIRP
GRATING
350-SLIT
NONLINEAR
CHIRP
GRATING
I
y
-x
(a)
(b)
(c)
(d)
0
-5
-10
-15
-20
-25
30
-50
-100
-150
-200
I: INTENSITY (dB)
x: x-DISPLACEMENT FROM FOCUS (microns)
y: y-DISPLACEMENT FROM FOCUS (microns)

FIGURE 5

FIGURE 6.

Experimental and theoretical logarithmic intensity responses of the 200–slit nonlinear grating across a wide (10 mm) field in the plane of the first order focus. Note (a) that the first order focus derives from the +1 diffraction order of the grating and (b) that the straight through 'spurious' transmission derives from the zeroth diffraction order. The other 'spurious' features in this figure derive from higher orders of diffraction. It is interesting to observe that the resemblance of these discrete features to the grating structure itself can be visualised as arising from pinhole camera images of the grating through the respective foci. In the case of the 350–slit gratings these orders run into each other making assignment of individual features difficult. In the theoretical plot no account has been taken of the element factor of the individual slits or polarisation effects. These account for the differences in intensity between experiment and theory.

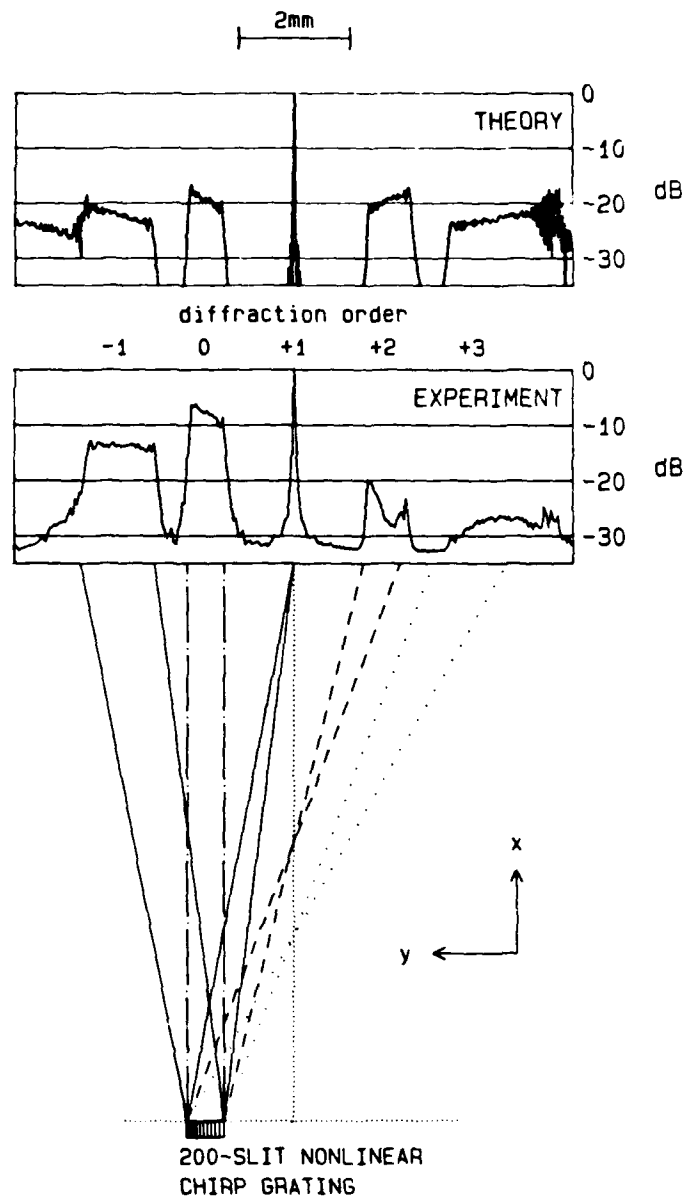
2mm
THEORY
0
-10
-20
-30
dB
diffraction order
-1
0
+1
+2
+3
EXPERIMENT
0
-10
-20
-30
dB
x
y
200-SLIT NONLINEAR
CHIRP GRATING

FIGURE 6

FIGURE 7.

Construction used to calculate the response of the gratings in the region of the first order focus for small deviations in x and y from the designed focus, F.

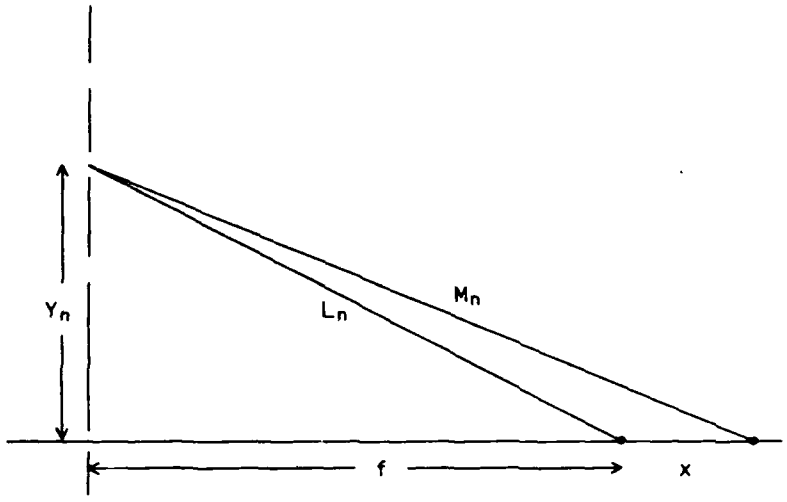


(a)

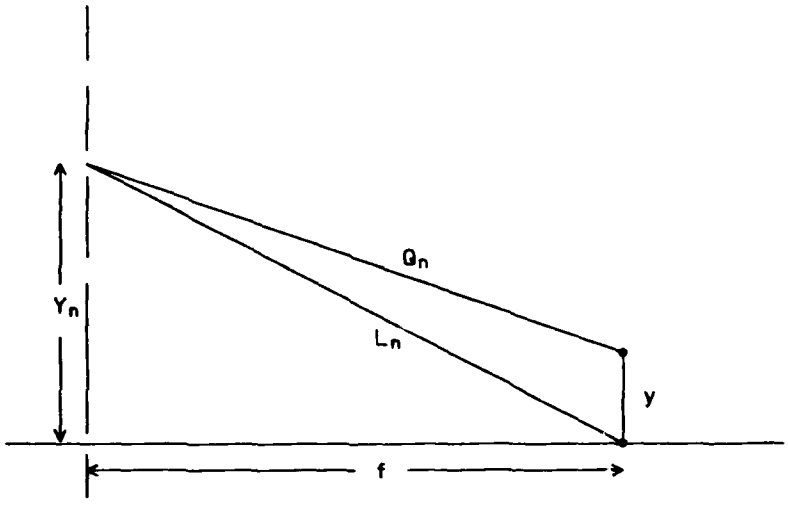


FIGURE 7 (b)

FIGURE 8.

Phasor diagrams to illustrate the origin of the filled-in nulls of the 350-slit nonlinear chirp grating of Figure 5. (a) This figure applies to a conventional diffraction grating at the first null of its sinc-function response, when the individual phasors span $2\pi$ and combine to give a vanishing resultant. (b) the corresponding phasor diagram for a 350-slit nonlinear chirp grating with constant slit width, W, showing a reduced, but non-vanishing resultant when the phasors span the range $0 - 2\pi$. This actual figure applies to $y = 2.7$ $\mu$m in Figure 5(c).

FIGURE 9.

Plan view of the formation of the far-field Fraunhofer pattern of a chirp grating, with its approximately rectangular response in the ±1 grating orders. The lens in this figure is used to relay the far field pattern to its focal plane. Typical experimental far field patterns for the 0, ±1 diffraction orders are shown to the right of this figure. Linear measures of the various intensity profiles are plotted in the x-direction (the ±1 diffraction order data are plotted on a scale expanded by 50 times compared to that for the zeroth order data). These results are discussed in more detail in reference 11.

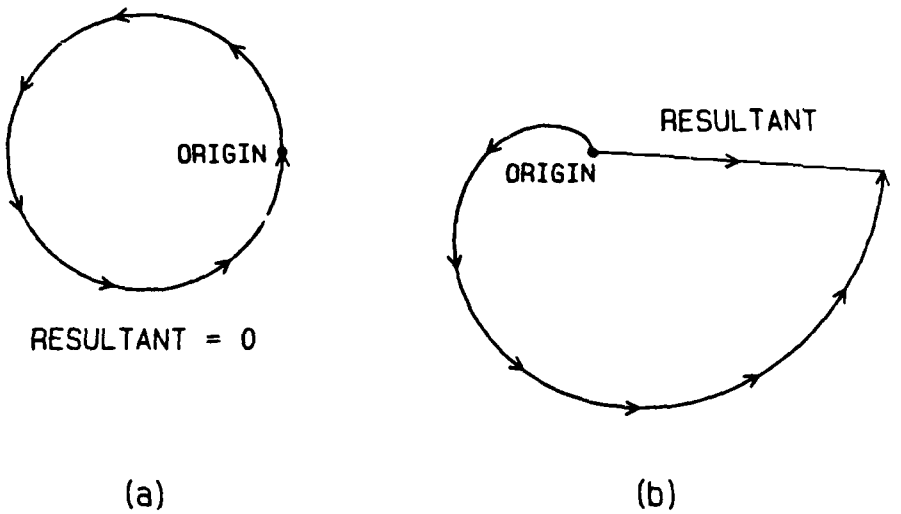


FIGURE 8

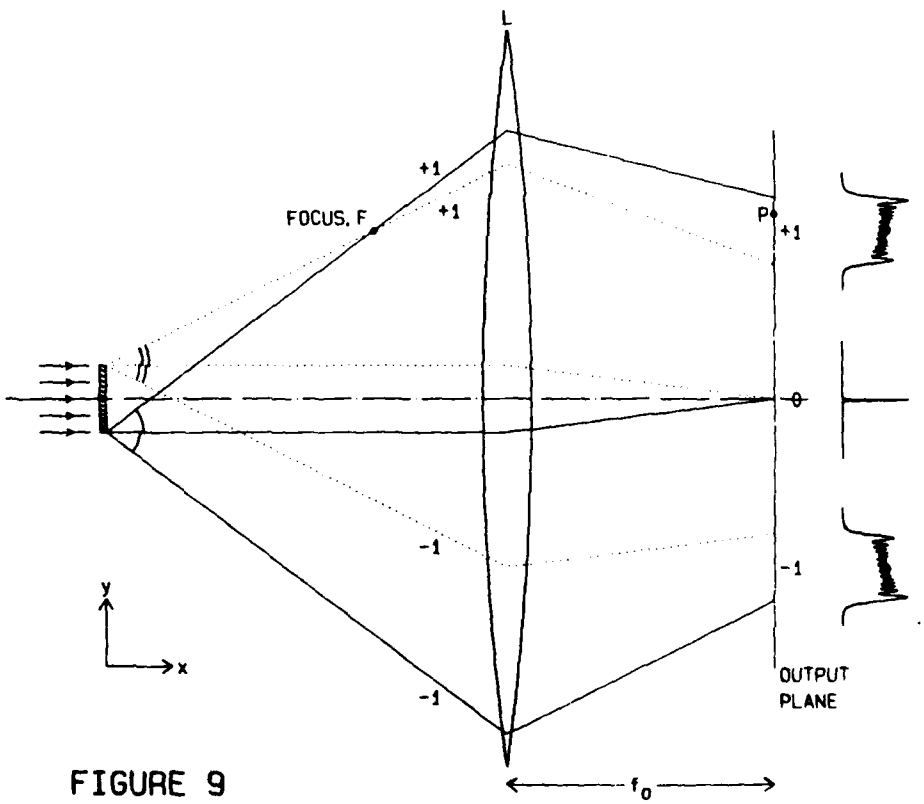


FIGURE 9

FIGURE A1.

Calculated focussing properties of various 1-sided and 2-sided grating structures. The perspective is obtained by adding a linear measure of the optical intensity to the x-coordinate. In (d) the scale for the optical intensity has been increased by a factor of approximately 4 relative to (a), (b) and (c) in order to make the degraded focus at ($\Delta x = -60\mu m$, $\Delta y = 0$) visible.

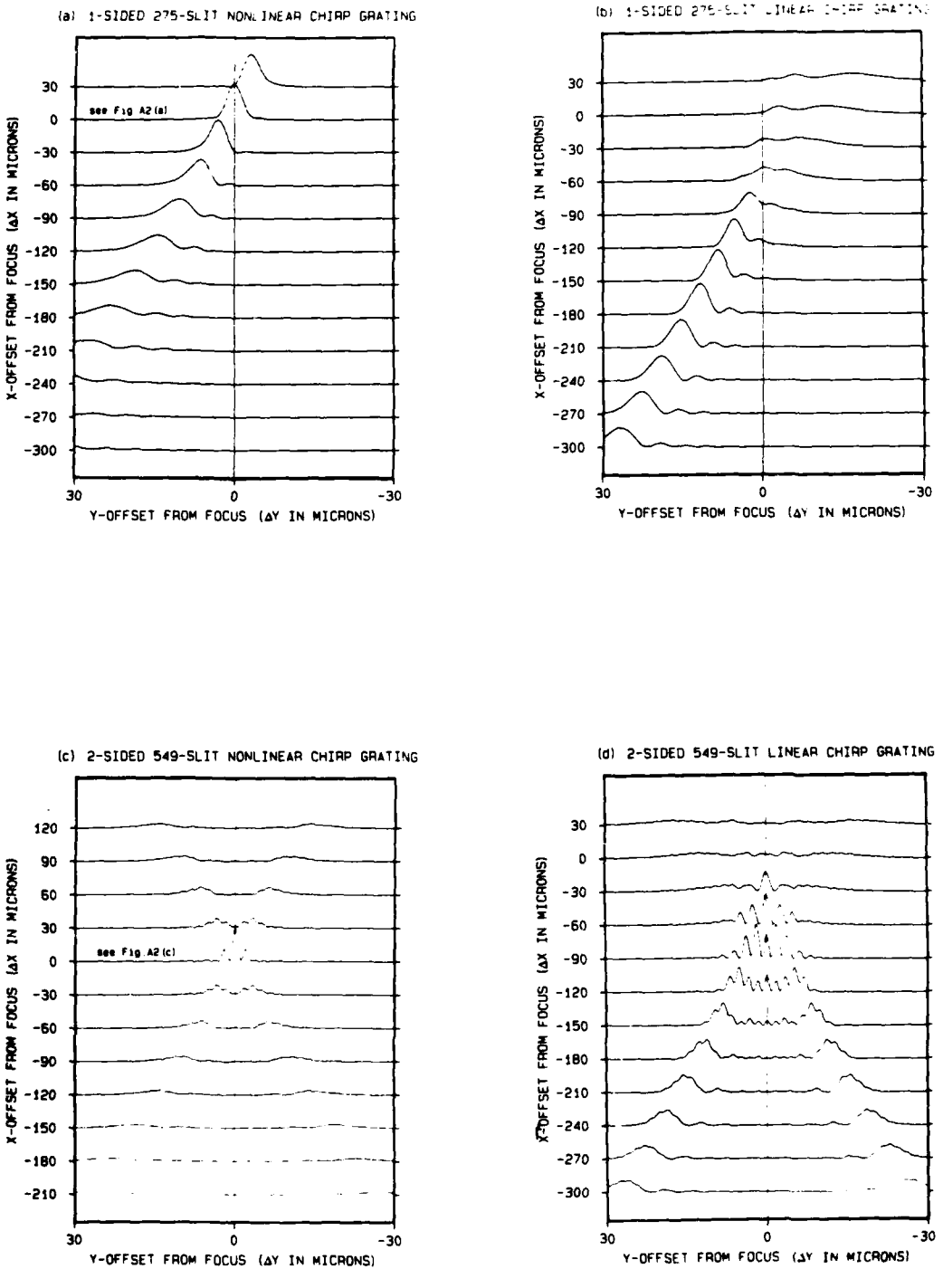
(a) 1-SIDED 275-SLIT NONLINEAR CHIRP GRATING
(b) 1-SIDED 275-SLIT LINEAR CHIRP GRATING
(c) 2-SIDED 549-SLIT NONLINEAR CHIRP GRATING
(d) 2-SIDED 549-SLIT LINEAR CHIRP GRATING
see Fig A2(a)
see Fig A2(c)
X-OFFSET FROM FOCUS (ΔX IN MICRONS)
Y-OFFSET FROM FOCUS (ΔY IN MICRONS)
30
0
-30
-60
-90
-120
-150
-180
-210
-240
-270
-300
120

FIGURE A1

FIGURE A2.

Detailed plots of the fields in the focal planes of various grating structures displayed on a logarithmic scale.

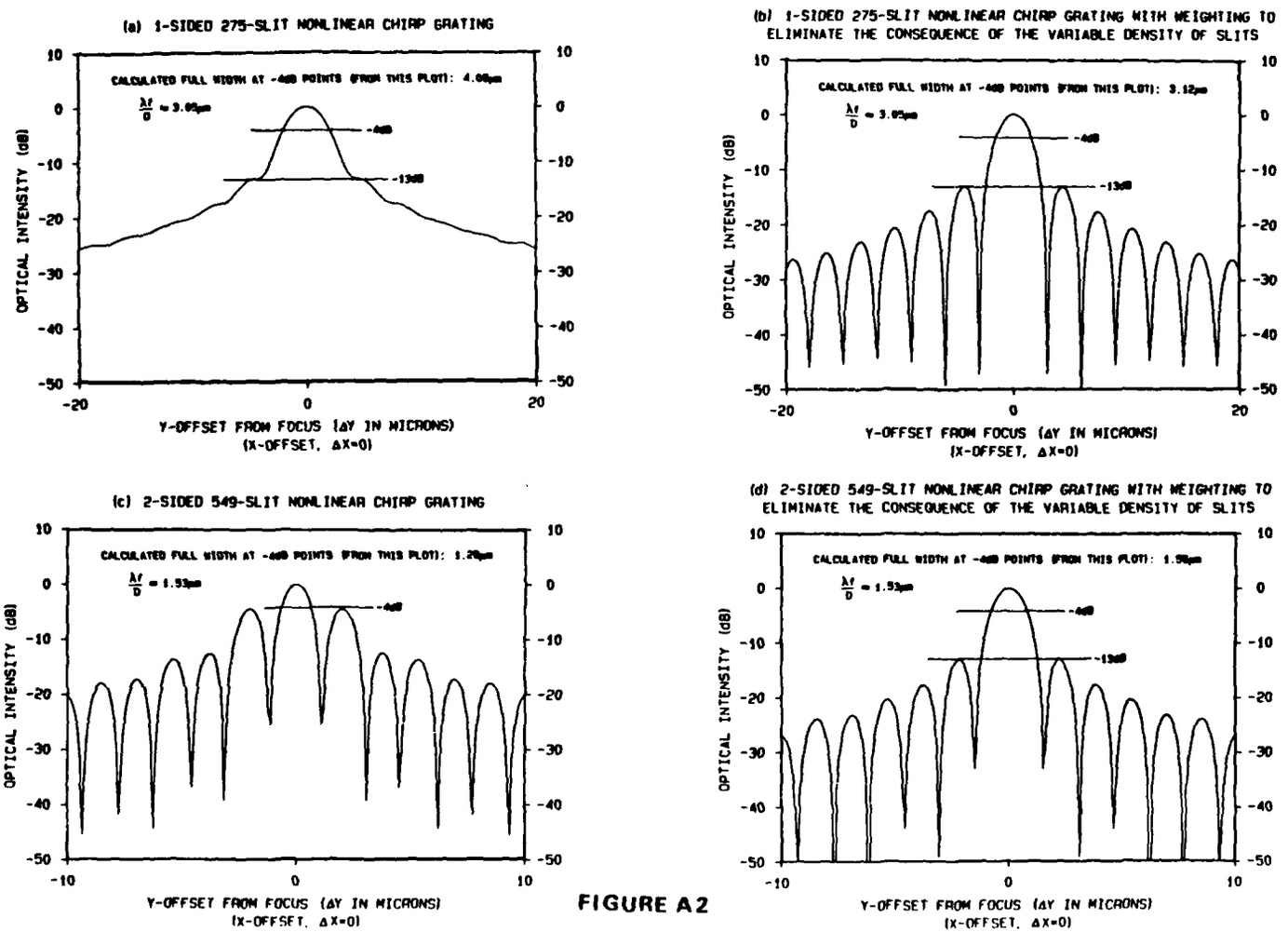
(a) 1-SIDED 275-SLIT NONLINEAR CHIRP GRATING
CALCULATED FULL WIDTH AT -4dB POINTS (FROM THIS PLOT): 4.08μm
λf/D = 3.05μm
-4dB
-13dB
OPTICAL INTENSITY (dB)
Y-OFFSET FROM FOCUS (ΔY IN MICRONS)
(X-OFFSET, ΔX=0)
(b) 1-SIDED 275-SLIT NONLINEAR CHIRP GRATING WITH WEIGHTING TO ELIMINATE THE CONSEQUENCE OF THE VARIABLE DENSITY OF SLITS
CALCULATED FULL WIDTH AT -4dB POINTS (FROM THIS PLOT): 3.12μm
λf/D = 3.05μm
-4dB
-13dB
OPTICAL INTENSITY (dB)
Y-OFFSET FROM FOCUS (ΔY IN MICRONS)
(X-OFFSET, ΔX=0)
(c) 2-SIDED 549-SLIT NONLINEAR CHIRP GRATING
CALCULATED FULL WIDTH AT -4dB POINTS (FROM THIS PLOT): 1.20μm
λf/D = 1.93μm
-4dB
OPTICAL INTENSITY (dB)
Y-OFFSET FROM FOCUS (ΔY IN MICRONS)
(X-OFFSET, ΔX=0)
(d) 2-SIDED 549-SLIT NONLINEAR CHIRP GRATING WITH WEIGHTING TO ELIMINATE THE CONSEQUENCE OF THE VARIABLE DENSITY OF SLITS
CALCULATED FULL WIDTH AT -4dB POINTS (FROM THIS PLOT): 1.56μm
λf/D = 1.93μm
-4dB
-13dB
OPTICAL INTENSITY (dB)
Y-OFFSET FROM FOCUS (ΔY IN MICRONS)
(X-OFFSET, ΔX=0)

FIGURE A2

DOCUMENT CONTROL SHEET

Overall security classification of sheet ..... UNCLASSIFIED .....

(As far as possible this sheet should contain only unclassified information. If it is necessary to enter classified information, the box concerned must be marked to indicate the classification eg (R) (C) or (S) )

| 1. DRIC Reference (if known) | 2. Originator's Reference | 3. Agency Reference | 4. Report Security Classification |
|---|---|---|---|
| | MEMO 4129 | | U/C |

| 5. Originator's Code (if known) | 6. Originator (Corporate Author) Name and Location |
|---|---|
| 778400 | ROYAL SIGNALS & RADAR ESTABLISHMENT<br>ST ANDREWS ROAD, GREAT MALVERN,<br>WORCESTERSHIRE WR14 3PS |
| 5a. Sponsoring Agency's Code (if known) | 6a. Sponsoring Agency (Contract Authority) Name and Location |

7. Title Theoretical and experimental investigation of linear and nonlinear focussing

7a. Title in Foreign Language (in the case of translations)

7b. Presented at (for conference papers) Title, place and date of conference

| 8. Author 1 Surname, initials | 9(a) Author 2 | 9(b) Authors 3,4... | 10. Date | pp. ref. |
|---|---|---|---|---|
| LEWIS M F | WEST C L | | 6.1988 | 28 |

| 11. Contract Number | 12. Period | 13. Project | 14. Other Reference |
|---|---|---|---|
| | | | |

15. Distribution statement

Descriptors (or keywords)

continue on separate piece of paper

Abstract In the past the focussing properties of chirped grating structures have been investigated in various disciplines including optics, acousto-optics and acoustics. In this paper we present the results of a detailed theoretical and experimental study of one such structure, namely the chirped optical diffraction grating, although many of the conclusions are of more general validity. We derive some useful fundamental properties of such focussing gratings, and show that to first order their behaviour is similar to that of various other classical components such as focussing lenses, grating spectrometers, and matched filters for chirped waveforms. However we also describe a fascinating range of second-order differences in behaviour, for example concerning the physical locations of the multiple

/cont .. /foci, and

foci, and the sidelobe structures within and perpendicular to the focal plane. For devices of large numerical aperture we demonstrate the advantages of using a non-linear chirp grating structure, eg for sidelobe suppression in the focal plane, and point out that surface acoustic wave (SAW) techniques can be used to generate the non-linear chirp waveforms necessary to implement such gratings in acousto-optic devices.